Journal of Power Sources 250 (2014) 250–256

Contents lists available at ScienceDirect

Journal of Power Sources

journal homepage: www.elsevier.com/locate/jpowsour

Nickel–cobalt hydroxide nanosheets arrays on Ni foam for pseudocapacitor applications

Jun Pu, Yao Tong, Shubo Wang, Enhong Sheng, Zhenghua Wang*

Key Laboratory of Functional Molecular Solids, Ministry of Education, College of Chemistry and Materials Science, Anhui Normal University, Wuhu 241000, PR China

HIGHLIGHTS

- Nickel–cobalt LDHs nanosheets was directly deposited on Ni foam using a facile hydrothermal method.
- LDHs–Ni foam could be used as binder-free electrode.
- Exhibited a high specific capacitance of 1734 F g^{-1} at 6 A g^{-1}.
- Remarkable specific capacitance at a high current density.

GRAPHICAL ABSTRACT

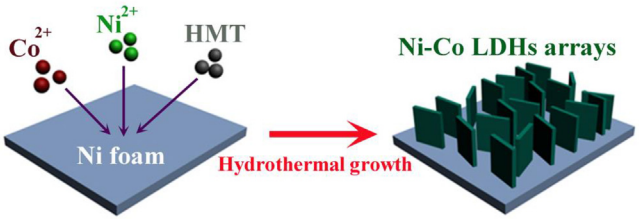

ARTICLE INFO

Article history:
Received 18 September 2013
Received in revised form
12 October 2013
Accepted 24 October 2013
Available online 19 November 2013

Keywords:
Layered double hydroxides
Supercapacitors
Binder-free
Ni foam

ABSTRACT

Vertically aligned nickel–cobalt layered double hydroxides (LDHs) nanosheets as electroactive materials are directly deposited on Ni foam substrate using a facile hydrothermal method. The Ni–Co LDHs nanosheets are interlaced on the substrate with an average thickness of about 20 nm. Galvanostatic charge–discharge measurement reveals that the LDHs–Ni foam binder-free electrode has an impressive specific capacitance as high as 1734 F g^{-1} at 6 A g^{-1} in 3 M KOH solution. It also shows a remarkable specific capacitance of up to 1146 F g^{-1} at a high current density of 30 A g^{-1}.

1. Introduction

With the development of human society, a large amount of energy sources have been consumed, such as coal, petroleum, natural gas, nuclear fission power and nuclear fusion power. However, under the circumstances, the quantity of energy sources is limited, unlimited usage of energy sources results in energy crisis, and also accompanied with environmental pollution. Therefore, the development of new energy storage devices becomes an urgent event. Supercapacitors, also called electrochemical capacitors are considered as promising candidate for energy storage because of their low cost, high power density, high dynamic of charge propagation and long durability [1–7].

The working mechanisms of supercapacitors are commonly divided into two types: charge separation at the electrode–electrolyte interface and redox reactions of the electroactive materials [8]. The pseudocapacitance (belong to the former) usually contains transition metal oxides or hydroxides as the electrode materials. The specific capacitance of pseudocapacitance is higher than that of the electrical double layer capacitors (EDLC, belong to the latter) that made of carbonaceous materials [9,10]. Among the well known pseudocapacitor materials, RuO_2 is widely studied as a wonderful electrode material with very high specific capacitance [11], but its high cost and low abundance hamper its practical application. Other transition metal oxides such as Mn_3O_4 [12], Fe_3O_4 [13], SnO_2 [14], Co_3O_4 [15], and NiO [16] are studied as the electrode material

* Corresponding author. Tel.: +86 553 3869303; fax: +86 553 3869302.
E-mail address: zhwang@mail.ahnu.edu.cn (Z. Wang).

0378-7753/$ – see front matter © 2013 Elsevier B.V. All rights reserved.
http://dx.doi.org/10.1016/j.jpowsour.2013.10.108

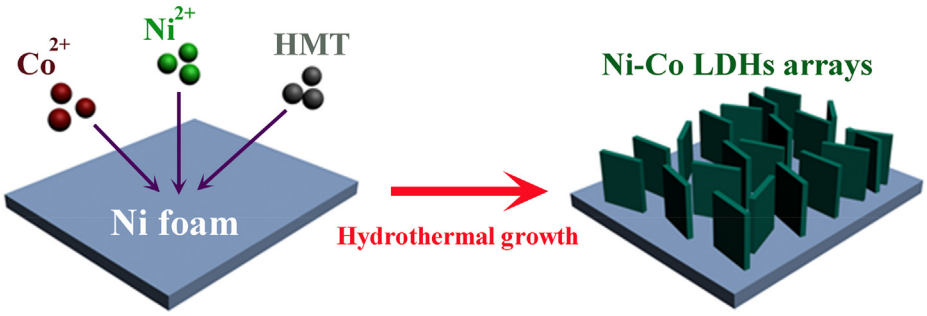

Scheme 1. Schematic illustration of the fabrication process of nickel–cobalt LDHs nanosheets.

for pseudocapacitors. However, these electrode materials show limited energy density than RuO_2. The exploration of electrode materials with higher power performance and low cost for pseudocapacitors is still of great importance.

Among the multitudinous materials for supercapacitors, hydroxides have been extensively researched due to their high capacitance, simple synthesis process and low cost. For instance, Wang et al. synthesized pompon like β-$Ni(OH)_2$ hollow microspheres that showed a capacitance of 1028.5 F g^{-1} at a current density of 2.2 A g^{-1} [17]. Dubal et al. reported $Ni(OH)_2$ thin films that prepared by a chemical bath deposition method, and revealed a capacitance of 462 F g^{-1} [18]. Hsu et al. prepared mesoporous Ni–Co hydroxides that have a capacitance of 636 F g^{-1} at 2 A g^{-1} [19]. These researches suggest that hydroxides are good candidate for supercapacitors electrode material.

Over the past ten years, the growth of electrode materials directly on conductive substrates as supercapacitors electrode has attracted more and more attentions because such a binder-free method can improve the electrochemical performance of supercapacitors. Cu conductive substrates, carbon fiber paper, Ti foil, stainless steel foil and Ni foam have been used as the conductive substrates [7,20–22]. The ion transportation can be enhanced and the electrode occupies smaller spaces when Ni foam was used as the conductive substrates for supercapacitors [9,23,24]. For instance, Zhang et al. have prepared ultrathin mesoporous Co_3O_4 nanosheet arrays on Ni foam with a high specific capacitance of 2735 F g^{-1} at 2 A g^{-1} [25]. Lou et al. have obtained ultrathin mesoporous $NiCo_2O_4$ nanosheets supported on Ni foam as advanced electrodes for supercapacitors, and an ultrahigh specific capacitance of 2010 F g^{-1} at 2 A g^{-1} was achieved [26]. Up to now, to the best of our knowledge, reports on Ni–Co LDHs grown on Ni foam for supercapacitors are still few. A recent study by Ahn et al. showed that Ni–Co LDHs nanorod arrays on stainless steel substrate have a capacitance of 456 F g^{-1} [27]. Herein, we report a facile hydrothermal method to grow ultrathin Ni–Co LDHs nanosheets on Ni foam. The galvanostatic charge–discharge test shows that the Ni–Co LDHs nanosheets have a high capacitance of 1734 F g^{-1} at a current density of 6 A g^{-1} in 3 M KOH solution.

2. Experimental

All the chemicals were of analytical grade, and were used without further purification.

2.1. Preparation of Ni–Co LDHs nanosheets

Typically, 0.582 g of $Co(NO_3)_2{\cdot}6H_2O$ (2 mmol), 0.582 g of $Ni(NO_3)_2{\cdot}6H_2O$ (2 mmol) and 1.12 g of hexamethylenetetramine (HMT) were dissolved in 30 mL distilled water under stirring to form a clear solution, and then the solution was transferred into a 40 mL Teflon-lined stainless-steel autoclave. A piece of clean Ni foam (2 cm × 3 cm) was treated with dilute hydrochloric acid, ethanol and distilled water in turn, and then was immersed into the above solution. The autoclave was sealed and heated at 100 °C for 10 h, then cooled to room temperature naturally. The Ni foam coated with Ni–Co LDHs nanosheets were rinsed under ultrasonication, and dried at 60 °C for 2 h. The mass of Ni foam before and after loading of Ni–Co LDHs nanosheets are 0.1878 g and 0.1958 g, respectively. The mass of Ni–Co LDHs nanosheets is 0.008 g and the loading of Ni–Co LDHs nanosheets is about 1.33 mg cm^{-2}. The typical fabrication procedure is shown in Scheme 1.

For comparison, $Co(OH)_2$ and $Ni(OH)_2$ nanosheets on Ni foam were also synthesized in the same way. The loading of $Co(OH)_2$ and $Ni(OH)_2$ nanosheets on Ni foam are 1.30 and 1.35 mg cm^{-2}, respectively.

2.2. Material characterization

The as-prepared product was characterized by X-ray powder diffraction (XRD, Philips X'pert PRO MPD diffractometer) with Cu Kα radiation (λ = 0.15406 nm) at a scanning rate of 0.05° s^{-1}. The field emission scanning electron microscopy (FESEM) images and energy dispersive X-ray spectrometer (EDX) were taken with a Hitachi S-4800 scanning electron microscope equipped with energy dispersive X-ray analysis system. Transmission electron microscopy (TEM) images were recorded on a FEI Tecnai G^2 20 high-resolution transmission electron microscope performed at an

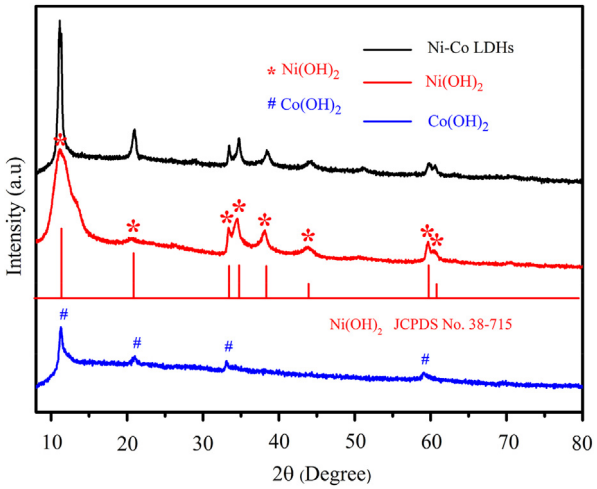

Fig. 1. XRD patterns of the $Ni(OH)_2$, $Co(OH)_2$ and Ni–Co LDHs composite nanosheets.

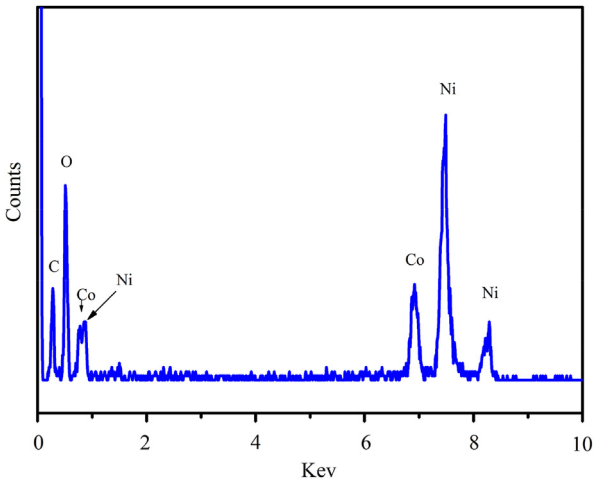

Fig. 2. EDX spectrum of the Ni–Co LDHs composite nanosheets.

acceleration voltage of 200 kV. X-ray photoelectron spectra (XPS) were recorded on an ESCALab MKII X-ray photoelectron spectrometer with nonmonochromatized Mg Kα X-ray as the excitation source. The binding energies in XPS analysis were corrected by referencing C 1s to 284.60 eV.

2.3. Electrochemical measurements

Electrochemical measurements were performed on an electrochemical working station (CHI660D, ChenHua Instruments Co. Ltd., Shanghai). A three electrode experimental setup taking a 3 M KOH aqueous solution as electrolyte was used in cyclic voltammetry (CV) and galvanostatic charge–discharge measurements. Here, the Ni–Co LDHs nanosheets loaded Ni foam (1.0 cm × 1.0 cm) directly acted as the working electrode, platinum wire and saturated calomel electrode (SCE) acted as the counter and reference electrodes, respectively.

The specific capacitance (C) of the electrode can be evaluated according to the following equation [28].

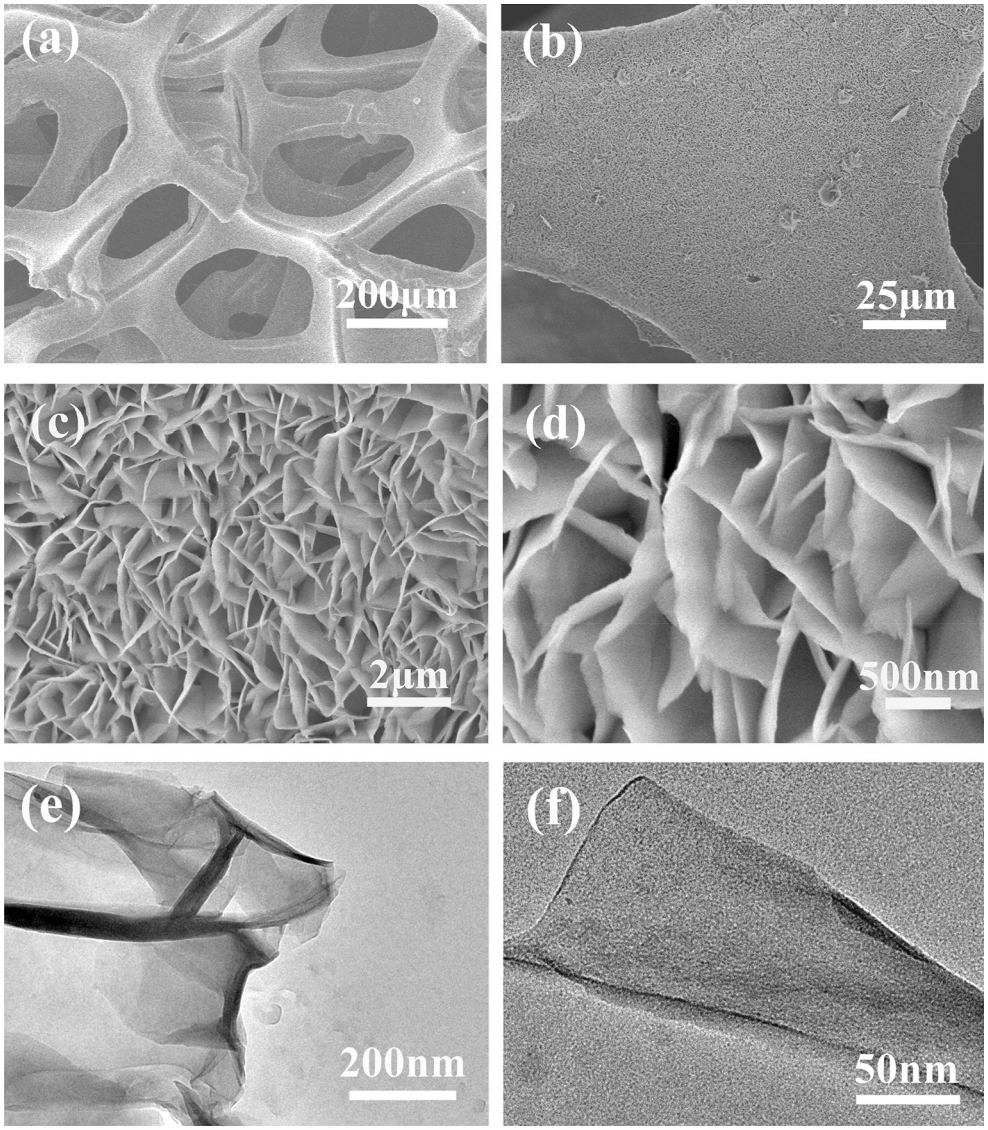

Fig. 3. (a) FESEM image of Ni foam; (b) FESEM image of Ni foam with Ni–Co LDHs nanosheets arrays grown by a hydrothermal process; (c,d) FESEM images of the Ni–Co LDHs nanosheets arrays on Ni foam; (e,f) TEM images of the Ni–Co LDHs nanosheets.

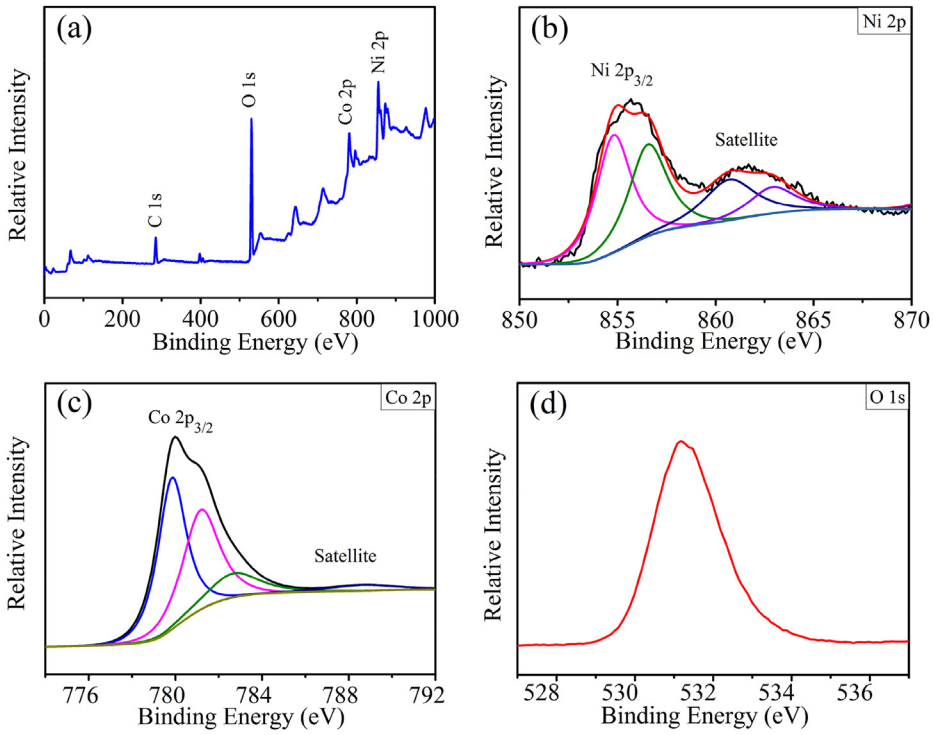

Fig. 4. XPS spectra of the sample: (a) the survey spectra, (b) core level spectra of the Ni $2p_{3/2}$ region, (c) core level spectra of the Co $2p_{3/2}$ region, and (d) core level spectra of the O 1s region.

$$C = \frac{I \times \Delta t}{m \times \Delta V} \quad (1)$$

where C (F g^{-1}) is the specific capacitance of the electrode based on the mass of active materials, I (A) is the current during discharge process, Δt (s) is the discharge time, ΔV (V) is the potential window (here $\Delta V = 0.45$ V), m (g) is the mass of active materials.

3. Results and discussion

Powder X-ray diffraction (XRD) was performed to characterize the crystalline structures of the prepared nickel–cobalt binary hydroxides, $Ni(OH)_2$ and $Co(OH)_2$, which are illustrated in Fig. 1. The diffraction peaks of the obtained $Ni(OH)_2$ sample can be indexed as rhombohedral phase α-$Ni(OH)_2$ (JCPDS No. 38-715), and the peaks of the $Co(OH)_2$ sample can be indexed as α-$Co(OH)_2$ [29]. As seen from the pattern of Ni–Co LDHs nanosheets, the XRD pattern consists of a mixture of both $Co(OH)_2$ and $Ni(OH)_2$ phases. No peaks arising from impurities can be found, indicating the composite materials were successfully synthesized.

The composition of the synthesized nanosheets was further examined by energy dispersive X-ray spectrometer (EDX), as shown in Fig. 2. Nickel and cobalt elements together with oxygen element are present, which is in agreement with the composition of Ni–Co LDHs. Hydrogen element is not present because it can not be detected by EDX. Carbon element is come from the carbon paste. No other redundant element can be found in the spectrum.

The morphology of the prepared samples was characterized by FESEM. Fig. 3a shows a FESEM image of the Ni foam substrate, which present a three dimensional (3D) network structure with smooth surfaces. After hydrothermal growth of Ni–Co LDHs on the substrate, the Ni foam turn from gray into green. FESEM observation shows that the surfaces of Ni foam are covered with plenty of ordered nanosheets, as shown in Fig. 3b. The detailed morphology of the as-synthesized Ni–Co LDHs is shown in Fig. 3c and d. The nanosheets are interconnected with each other and interlaced like petals. The thickness of these nanosheets is uniform, with an average size of about 20 nm. The Ni–Co LDHs nanosheets arrays on Ni foam formed the network structures, which is favorable for the electron transportation among the materials and improve their capacitive performances [30]. Typical TEM images of the nanosheets display sheet-like morphology, as shown in Fig. 3e and f. The transparent feature of the nanosheets indicates their ultrathin nature.

The chemical bonding states of each element on the surface of the Ni–Co LDHs nanosheets were evaluated by XPS technique, as shown in Fig. 4. A typical survey XPS spectrum of the Ni–Co LDHs is illustrated in Fig. 4a, in which Ni, Co, O and C elements are present. The C element is due to exposure to the air. According to the report by Smart et al. [31], the main peaks at 855.8 eV, 780.7 eV and other all fitted peaks in Ni $2p_{3/2}$ and Co $2p_{3/2}$ spectra (Fig. 4b and c) should be assigned to Ni^{2+} and Co^{2+} in Ni–Co LDHs, respectively. Fig. 4d shows the XPS spectrum of O 1s, the peak at 531.1 eV can be related to hydroxyl ions [32].

Cyclic voltammetry (CV) curves were measured at different potential sweep rates to reflect the electrochemical properties of the Ni–Co LDHs nanosheets on Ni foam that directly applied as self-supported electrode, and the results are shown in Fig. 5a. A pair of redox peaks with an anodic peak at around 0.15 V and a cathodic peak at about 0.32 V is clearly observed when the scan rate is 10 mV s^{-1}. In addition, with the increase of scan rate, the height of the peak currents varies and a progressive shift of the peaks to higher potential was observed. The mechanism of electrochemical reactions may be explained by the diffusion of OH^- ions into the Ni–Co LDHs nanosheets. At low scan rates, the movement of OH^- ions is slower than that at high scan rates, and the active materials have a higher utilization ratio [33]. All the CVs are almost symmetric,

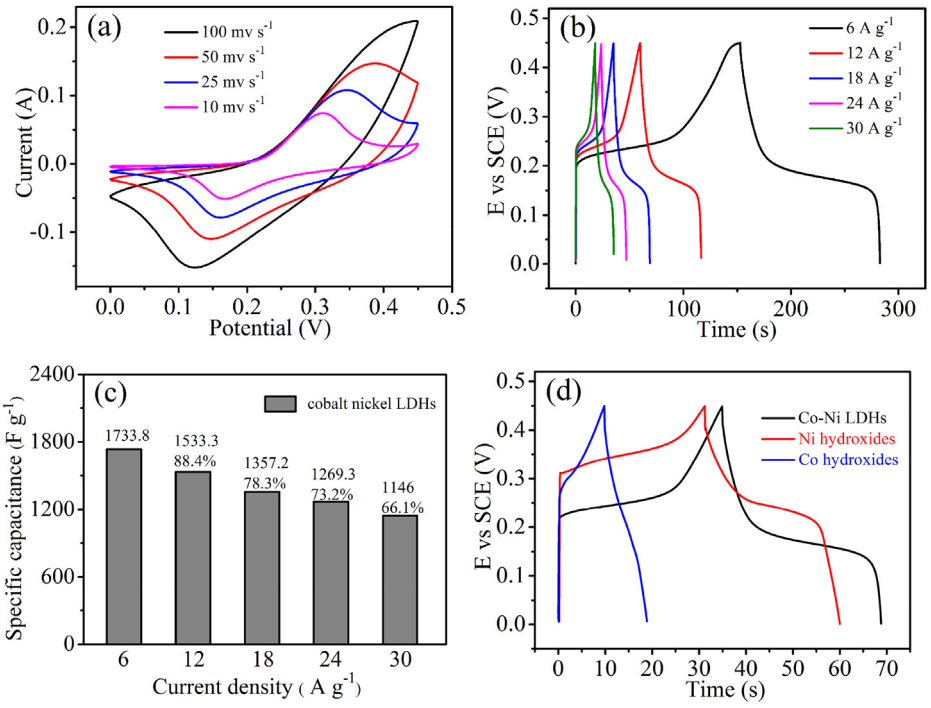

Fig. 5. (a) CV curves of the Ni–Co LDHs nanosheets arrays at various scan rates; (b) galvanostatic charge–discharge curves of Ni–Co LDHs electrode measured at various current densities; (c) charge–discharge curves of $Ni(OH)_2$, $Co(OH)_2$ and Ni–Co LDHs arrays at 18 A g^{-1}; (d) specific capacitance of LDHs electrode at different discharge current densities.

which suggest the fine reversibility of the oxidation and reduction processes. The following Faradaic reactions of $Co(OH)_2$ and $Ni(OH)_2$ may occur during the electrochemical reactions [34,35].

$$Co(OH)_2 + OH^- \leftrightarrow CoOOH + H_2O + e^- \quad (2)$$

$$CoOOH + OH^- \leftrightarrow CoO_2 + H_2O + e^- \quad (3)$$

$$Ni(OH)_2 + OH^- \leftrightarrow NiOOH + H_2O + e^- \quad (4)$$

The good performance of Ni–Co LDHs nanosheets arrays on Ni foam can be attributed to the following aspects: (1) The nanosheets with network structures not only provide more sites for the adsorption of ions, but also contribute efficient pathways for charge transport [36]. (2) The interconnected networks of Ni–Co LDHs directly anchored on Ni foam can afford intimate electric contact of active materials to conductive substrates [37]. As shown in Scheme 2, the 3D structure provides deep electrolyte penetration for electrons and hydroxyl ions during the period of redox reaction.

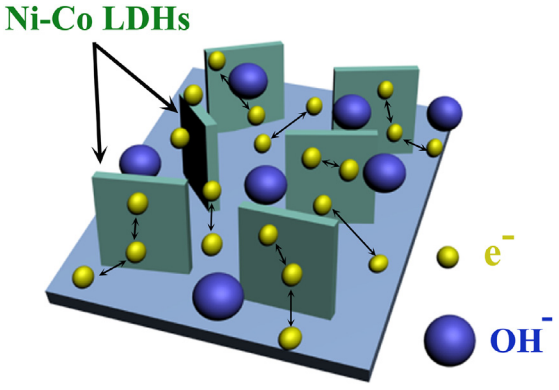

Scheme 2. Schematic illustration of the transportation of species on nickel–cobalt LDHs nanosheets in 3 M KOH solution.

The galvanostatic charge–discharge of Ni–Co LDHs between 0 and 0.45 V at a set of current densities show bamboo hat-like shapes reflect good capacitive performance, as shown in Fig. 5b. A symmetric shape during the charge–discharge process is observed, indicating their good supercapacitive behaviors. All of the graphs have voltage plateaus between 0.15 V and 0.25 V, which are different from the curves of electrical double layer capacitors with two straight lines. The result shows that with the increase in current density, the discharge time reduces. The relationship between specific capacitance and current density is illustrated in Fig. 5c. The specific capacitance that calculated from formula (1) can achieve a maximum of 1734 F g^{-1} at 6 A g^{-1}. What's more, the Ni–Co LDHs nanosheets arrays show 66.1% capacitance retention from 6 A g^{-1} to 30 A g^{-1}. As a contrast, Fig. 5d depicts the galvanostatic charge–discharge tests of $Co(OH)_2$, $Ni(OH)_2$ and Ni–Co LDHs that performed with an applied constant current density of 18 A g^{-1}. The capacitance of the Ni–Co LDHs is thus calculated to be 1357 F g^{-1}, higher than that of the pure $Ni(OH)_2$ (1220 F g^{-1}) and $Co(OH)_2$ (341 F g^{-1}). In comparison with the previously reported nickel–cobalt hydroxide nanorod arrays with a capacitance of 456 F g^{-1} [27], and the binary Ni–Co hydroxides with a capacitance of 632 F g^{-1} [38], the Ni–Co LDHs arrays on Ni foam also reveal superior capability.

In addition, cycling stability of the $Co(OH)_2$, $Ni(OH)_2$ and Ni–Co LDHs nanosheets arrays were investigated within 1000 cycles at a high current density of 18 A g^{-1}, as shown in Fig. 6a. The Ni–Co LDHs nanosheets show 86% capacitance retention, which is higher than $Co(OH)_2$ (80%), $Ni(OH)_2$ (78%), and previously reported donut-like $Ni(OH)_2$–$Co(OH)_2$ composites (84.7%) [39] and nickel–cobalt hydroxide on nickel-coated silicon microchannel plates (83.9%) [9]. According to the results, the Ni–Co LDHs demonstrates better cycling performances.

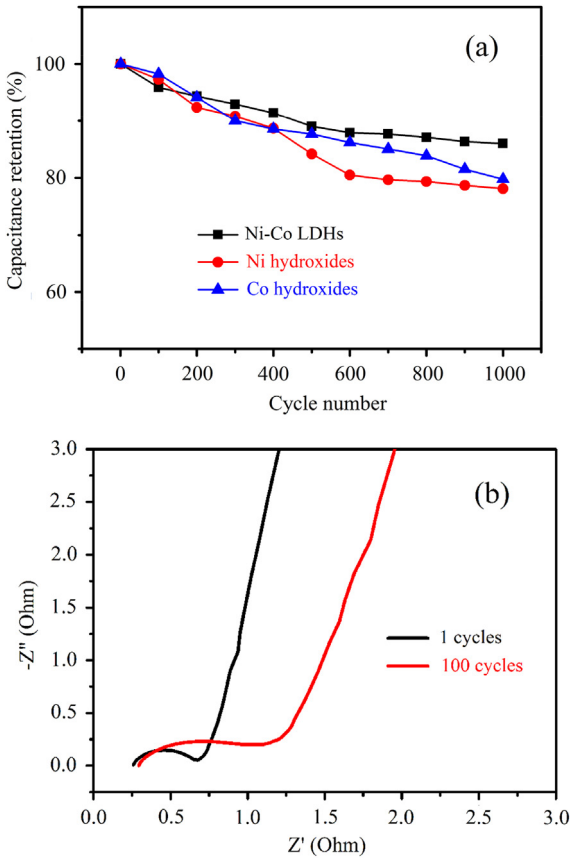

Fig. 6. (a) Stability test in terms of specific capacitance for $Ni(OH)_2$, $Co(OH)_2$ and Ni–Co LDHs nanosheets arrays; (b) Nyquist plots of Ni–Co LDHs nanosheets arrays supercapacitor cell.

Specific energy density (E) and specific power density (P) derived from galvanostatic tests can be calculated from the equations [3]:

$$E = \frac{1}{2}C\Delta V^2 \tag{5}$$

$$P = \frac{E}{\Delta t} \tag{6}$$

where E (Wh kg^{-1}) is the average energy density; C (F g^{-1}) is the specific capacitance; ΔV (V) is the potential window; P (kW kg^{-1}) is the average power density and Δt (s) is the discharge time.

Table 1 indicates energy density and power density versus current density for the Ni–Co LDHs sample. The specific energy is found to decrease from 48.8 to 32.2 Wh kg^{-1} when the current density increases from 6 to 30 A g^{-1}. More precisely, it has a high energy density of ca. 48.8 Wh kg^{-1} at a power density of ca. 1.4 kW kg^{-1} and a high power density of ca. 6.8 kW kg^{-1} at an energy density of ca. 32.2 Wh kg^{-1}.

Table 1
The energy density and power density versus different current densities of the Ni–Co LDHs sample.

Current density (A g^{-1})	6	12	18	24	30
Energy density (Wh kg^{-1})	48.8	43.1	38.2	35.7	32.2
Power density (kW kg^{-1})	1.4	2.7	4.1	5.4	6.8

The EIS, also known as Nyquist plot, shows the frequency response of the electrode–electrolyte system and is a plot of the imaginary component of the impedance against real component [40,41]. Fig. 6b displays the impedance responses of Ni–Co LDHs that was carried out at the open circuit potential in the frequency range of 100 kHz to 0.01 Hz. The plot is composed of partial semicircle and sloping straight lines, demonstrating that the electrode behaves more closely as an ideal capacitor. The small semicircle in high frequency domain almost perpendicular to the straight line in low frequency portion of the spectrum, show that the materials have nethermore charge transfer resistance, which agree well with cyclic voltammetry (CV) curves. The semicircle became larger after cycling for 100 times, and the values of charge transfer resistance for the Ni–Co LDHs at first cycle and 100 cycles are 0.75 Ω and 1.15 Ω, respectively. These results also reveal the enhancement of the charge-transfer resistance in the electrode reaction.

4. Conclusions

In summary, Ni–Co LDHs nanosheets arrays were successfully grown on Ni foam substrates by a convenient hydrothermal method and their performance in supercapacitors was studied. The Ni–Co LDHs nanosheets display excellent specific capacitance of 1734 F g^{-1} at 6 A g^{-1}. The capacitance retention of the Ni–Co LDHs in galvanostatic charge–discharge test after 1000 cycles was 86%, revealing better stability than that of the $Co(OH)_2$ and $Ni(OH)_2$. Therefore, the good electrochemical property of the Ni–Co LDHs nanosheets arrays will make them attractive for promising application in the field of supercapacitors.

Acknowledgments

Financial support from the National Natural Science Foundation of China (Project No. 21171006) is gratefully acknowledged.

References

[1] G.Q. Zhang, X.W. Lou, Adv. Mater. 25 (2013) 976–979.
[2] X.Y. Dong, L. Wang, D. Wang, C. Li, J. Jin, Langmuir 28 (2012) 293–298.
[3] X.Y. Chen, C. Chen, Z.J. Zhang, D.H. Xie, X. Deng, J.W. Liu, J. Power Sources 230 (2013) 50–58.
[4] I.H. Nam, S.M. Park, Gil-Pyo Kim, J.S. Park, J.H. Yi, Chem. Sci. 4 (2013) 1663–1667.
[5] D.Y. Zhai, B.H. Li, H.D. Du, G.Y. Gao, L. Gan, Y.B. He, Q.H. Yang, F.Y. Kang, Carbon 50 (2012) 5034–5043.
[6] L. Yu, G.Q. Zhang, C.Z. Yuan, X.W. Lou, Chem. Commun. 49 (2013) 137–139.
[7] L. Huang, D.C. Chen, Y. Ding, S. Feng, Z.L. Wang, M.L. Liu, Nano Lett. 13 (2013) 3135–3139.
[8] P. Simon, Y. Gogotsi, Nat. Mater. 7 (2008) 845–854.
[9] T. Liu, S.H. Xu, L.W. Wang, J.H. Chu, Q.J. Wang, X.R. Zhu, N.C. Bing, Paul K. Chu, J. Mater. Chem. 21 (2011) 19093–19100.
[10] P.M. Hallam, M.G. Mingot, D.K. Kampouris, C.E. Banks, RSC Adv. 2 (2012) 6672–6679.
[11] Z.H. Wang, Q. Sha, F.W. Zhang, J. Pu, W. Zhang, Cryst. Eng. Comm. 15 (2013) 5928–5934.
[12] H. Jiang, T. Zhao, C.Y. Yan, Jan Ma, C.Z. Li, Nanoscale 2 (2010) 2195–2198.
[13] J.B. Mu, B. Chen, Z.C. Guo, M.Y. Zhang, Z.Y. Zhang, P. Zhang, C.L. Shao, Y.C. Liu, Nanoscale 3 (2011) 5034–5040.
[14] R.K. Selvan, I. Perelshtein, N. Perkas, A. Gedanken, J. Phys. Chem. C 112 (2008) 1825–1830.
[15] S.L. Xiong, C.Z. Yuan, X.G. Zhang, B.J. Xi, Y.T. Qian, Chem. Eur. J. 15 (2009) 5320–5326.
[16] C.Y. Cao, W. Guo, Z.M. Cui, W.G. Song, W. Cai, J. Mater. Chem. 21 (2011) 3204–3209.
[17] Y. Wang, S.L. Gai, C.X. Li, F. He, M.L. Zhang, Y.D. Yan, P.P. Yang, Electrochim. Acta 90 (2013) 673–681.
[18] D.P. Dubal, V.J. Fulari, C.D. Lokhande, Micropor. Mesopor. Mater. 151 (2012) 511–516.
[19] H.Y. Hsu, K.H. Chang, R.R. Salunkhe, C.T. Hsu, C.C. Hu, Electrochim. Acta 94 (2013) 104–112.
[20] J. Liu, C.P. Liu, Y.L. Wan, W. Liu, Z.S. Ma, S.M. Ji, J.B. Wang, Y.C. Zhou, P. Hodgson, Y.C. Li, Cryst. Eng. Comm. 15 (2013) 1578–1585.

[21] G.Q. Zhang, H.B. Wu, H.E. Hoster, Mary B. Chan-Park, X.W. Lou, Energy Environ. Sci. 5 (2012) 9453–9456.
[22] V. Gupta, S. Gupta, N. Miura, J. Power Sources 175 (2008) 680–685.
[23] J. Li, Q.M. Yang, I. Zhitomirsky, J. Power Sources 185 (2008) 1569–1574.
[24] J. Jiang, Y.Y. Li, J.P. Liu, X.T. Huang, C.Z. Yuan, X.W. Lou, Adv. Mater. 24 (2012) 5166–5180.
[25] C.Z. Yuan, L. Yang, L.R. Hou, L.F. Shen, X.G. Zhang, X.W. Lou, Energy Environ. Sci. 5 (2012) 7883–7887.
[26] C.Z. Yuan, J.Y. Li, L.R. Hou, X.G. Zhang, L.F. Shen, X.W. Lou, Adv. Funct. Mater. 22 (2012) 4592–4597.
[27] R.R. Salunkhe, K.H. Jang, S.W. Lee, H. Ahn, RSC Adv. 2 (2012) 3190–3193.
[28] B. Xu, H. Duan, M. Chu, G.P. Cao, Y.S. Yang, J. Mater. Chem. A 1 (2013) 4565–4570.
[29] Z.A. Hu, Y.L. Xie, Y.X. Wang, H.Y. Wu, Y.Y. Yang, Z.Y. Zhang, Electrochim. Acta 54 (2009) 2737–2741.
[30] J.H. Zhong, A.L. Wang, G.R. Li, J.W. Wang, Y.N. Ou, Y.X. Tong, J. Mater. Chem. 22 (2012) 5656–5665.
[31] M.C. Biesingera, B.P. Payne, A.P. Grosvenor, L.W.M. Lau, A.R. Gerson, R.S.C. Smart, Appl. Surf. Sci. 257 (2011) 2717–2730.
[32] J.D. Dupin, D. Gonbeau, P. Vinatierb, A. Levasseur, Phys. Chem. Chem. Phys. 2 (2000) 1319–1324.
[33] M. Toupin, T. Brousse, D. Belanger, Chem. Mater. 14 (2002) 3946–3952.
[34] L.J. Xie, Z.G. Hu, C.X. Lv, G.H. Sun, J.L. Wang, Y.Q. Li, H.W. He, J. Wang, K.X. Li, Electrochim. Acta 78 (2012) 205–211.
[35] Z.R. Chang, Y.J. Zhao, Y.C. Ding, J. Power Sources 77 (1999) 69–73.
[36] H.M. Zheng, T. Zhai, M.H. Yu, S.L. Xie, C.L. Liang, W.X. Zhao, S.C. Wang, Z.S. Zhang, X.H. Lu, J. Mater. Chem. C 1 (2013) 225–229.
[37] X.H. Lu, X. Huang, S.L. Xie, T. Zhai, C.S. Wang, P. Zhang, M.H. Yu, W. Li, C.L. Liang, Y.X. Tong, J. Mater. Chem. 22 (2012) 13357–13364.
[38] B.P. Bastakoti, Y. Kamachi, H.S. Huang, L.C. Chen, K.C.W. Wu, Y. Yamauchi, Eur. J. Inorg. Chem. 2013 (2013) 39–43.
[39] J.X. Li, M. Yang, J.P. Wei, Z. Zhou, Nanoscale 4 (2012) 4498–4503.
[40] Z.Q. Niu, P.S. Luan, Q. Shao, H.B. Dong, J.Z. Li, J. Chen, D. Zhao, L. Cai, W.Y. Zhou, X.D. Chen, S.S. Xie, Energy Environ. Sci. 5 (2012) 8726–8733.
[41] X.Z. Wu, W. Xing, L. Zhang, S.P. Zhuo, J. Zhou, G.Q. Wang, S.Z. Qiao, Powder Technol. 224 (2012) 162–167.